J. Fluid Mech. (1982), *vol.* 118, *pp.* 285–304
Printed in Great Britain

Soliton models of long internal waves

By HARVEY SEGUR

Aeronautical Research Associates of Princeton, Inc.,
P.O. Box 2229, Princeton, New Jersey 08540, U.S.A.

AND J. L. HAMMACK†

Department of Civil Engineering, University of California,
Berkeley, California 94720, U.S.A.

(Received 5 May 1981 and in revised form 9 November 1981)

The Korteweg–de Vries (KdV) equation and the finite-depth equation of Joseph (1977) and Kubota, Ko & Dobbs (1978) both describe the evolution of long internal waves of small but finite amplitude, propagating in one direction. In this paper, both theories are tested experimentally by comparing measured and theoretical soliton shapes. The KdV equation predicts the shapes of our measured solitons with remarkable accuracy, much better than does the finite-depth equation. When carried to second-order, the finite-depth theory becomes about as accurate as (first-order) KdV theory for our experiments. However, second-order corrections to the finite-depth theory also identify a bound on the range of validity of that entire expansion. This range turns out to be rather small; it includes only about half of the experiments reported by Koop & Butler (1981).

1. Introduction

The evolution of long internal waves with small amplitudes in a stably stratified fluid is governed approximately by a linear wave equation, with small but cumulative corrections due to weak nonlinearity, dispersion and dissipation, and possibly to a slowly varying background. Several theoretical models exist which include various combinations of these cumulative effects. The purpose of this paper is to test two of these theoretical models experimentally in order to obtain some notion of their accuracy and range of validity.

The two theoretical models that we consider are weakly nonlinear and weakly dispersive: the Korteweg–de Vries (KdV) (1895) equation,

$$f_\tau + 6ff_\chi + f_{\chi\chi\chi} = 0, \tag{1}$$

and an equation due to Joseph (1977) and to Kubota, Ko & Dobbs (1978),

$$f_\tau + ff_\chi + T[f_{\chi\chi}] = 0, \tag{2a}$$

where

$$T[f] = -\frac{1}{2}\int_{-\infty}^{\infty} f(y)\coth\tfrac{1}{2}\pi(\chi - y)\,dy, \tag{2b}$$

and the integral is evaluated in the principal-value sense. The latter equation, which we will call the 'finite-depth equation', may be written in a variety of equivalent ways,

† Present address: Dept of Engng Sciences, University of Florida, Gainesville, Fla 32611.

of which (2) is perhaps the simplest. This list of equations could logically include an equation proposed by Benjamin (1967) and later derived by Ono (1975),

$$f_\tau + ff_\chi - H[f_{\chi\chi}] = 0, \tag{3}$$

where $H[\ ]$ is the Hilbert transform. However, we will not consider (3) because we have no experimental data in the range of parameters where (3) is valid.

It is well-known that the KdV equation describes the slow evolution of internal waves of fairly small amplitude that are long in comparison with the total fluid depth (see e.g. Benney 1966). However, this meaning of 'long' is overly restrictive because it excludes internal waves whose wavelengths may be comparable or even less than the total fluid depth, but which are much longer than the thickness of an appropriate thin layer defined by the background density distribution. For example, Osborne & Burch (1980) have observed internal waves in the Andaman Sea that seem to behave like KdV solitons, even though their observed wavelengths are only comparable to the total water depth.

As we will discuss in § 2, the derivation of (2) permits wavelengths comparable to the total fluid depth, provided only that they are much longer than the thickness of an appropriate thin layer. Thus, there is a sense in which (2) generalizes (1), and one might expect (2) to be at least as accurate as (1) in predicting experimental data.

We find the opposite to be true: for our data set, the predictions of (2) are always less accurate than those of (1). The finite-depth equation predicts the data accurately only in so far as it agrees with the KdV equation. This conclusion is based on our limited set of data, but Koop & Butler (1981) have reached substantially the same conclusion on the basis of independent experiments.

As we will show, the resolution of this paradox is as follows. Both (1) and (2) are derived from Euler's equations of motion by comparable asymptotic expansions. In each case, the solution of the equation, (1) or (2), provides the dominant term in the asymptotic expansion. However, in terms of allowable wave amplitudes, the range of validity of (2) is rather small; in fact, it is much smaller than that of (1). This limited range is found by carrying the expansion that leads to (2) to the next order, and comparing the second-order theory with experimental data.

Thus, under somewhat different conditions, both (1) and (2) predict the slow evolution of long internal waves of small amplitude as they travel in one direction. However, waves that are long enough to satisfy the requirements for (2) are not necessarily long enough for (1). On the other hand, waves that have amplitudes small enough to satisfy the requirements for (1) may lie outside the range of validity of (2).

2. Derivation of the equations

We consider a two-fluid configuration, in which a layer of lighter fluid overlies a layer of heavier fluid, resting on a horizontal impermeable bed in a constant gravitational field (see figure 1). This is the simplest configuration that supports internal gravity waves, and it is adequate to model the waves observed in our experiments, in those of Koop & Butler (1981), and in those of Osborne & Burch (1980). It excludes higher vertical modes, including those studied by Kubota *et al.* (1978). Therefore, our results cannot be compared directly with theirs, although the derivations themselves may be compared.

The problem of finding the two-dimensional, infinitesimal, irrotational disturbances admitted by two stably stratified layers of incompressible fluid in a constant gravitational field was discussed by Lamb (1932, §231). The velocity potentials in the upper and lower fluids may be written as

$$\phi_1 \sim (A \sinh kz + B \cosh kz) \exp ik[x - c(k)t],$$

$$\phi_2 \sim D \cosh k(z + h_2) \exp ik[x - c(k)t].$$

Here $c(k)$ must satisfy the linear dispersion relation

$$\left(\frac{kc^2}{g}\right)^2 [1 + (1-\Delta) T_1 T_2] - \frac{kc^2}{g}[T_1 + T_2] + \Delta T_1 T_2 = 0, \tag{4a}$$

where

$$\Delta = \frac{\rho_2 - \rho_1}{\rho_2}, \tag{4b}$$

$$T_i = \tanh kh_i \quad (i = 1, 2). \tag{4c}$$

In our experiments $\Delta \simeq 0{\cdot}05$; therefore, we will use the Boussinesq approximation ($\Delta \to 0$, but $g\Delta$ finite) to simplify results. Some generalizations to arbitrary Δ ($0 \leqslant \Delta \leqslant 1$) are mentioned below. For small Δ, the roots of (4*a*) are

$$c_s^2(k) = \frac{g}{k} \tanh k(h_1 + h_2) + O(\Delta) \quad \text{(surface waves)} \tag{5a}$$

$$c_i^2(k) = \frac{g\Delta T_1 T_2}{k(T_1 + T_2)} [1 + O(\Delta)] \quad \text{(internal waves)}. \tag{5b}$$

In the Boussinesq limit, these speeds always are distinct for a given k. Henceforth, we will let $\Delta \to 0$ (and $g \to \infty$), and retain only dominant terms.

A major difference between (1) and (2) is due to different approximations of (5*b*). The KdV limit is obtained by letting $k(h_1 + h_2) \to 0$, so that

$$c_s^2(0) = g(h_1 + h_2), \tag{6a}$$

$$c_i^2(0) = \frac{g\Delta h_1 h_2}{h_1 + h_2} \equiv c_0^2. \tag{6b}$$

The dispersive term in (1) corresponds to the first correction to (6*b*) for small $k(h_1 + h_2)$. On the other hand, the finite-depth limit amounts to $h_2/h_1 \to 0$, kh_1 finite, so that

$$c_i^2(0) = g\Delta h_2 \equiv \bar{c}^2. \tag{7}$$

The dispersive term in (2) corresponds to the first correction to (7) for small kh_2. Note that the speeds of the long infinitesimal waves in (6*b*) and (7) differ, unless we also require $h_2/h_1 \to 0$ in (6*b*).

2.1. *The KdV equation*

Aspects of KdV theory for long internal waves have been discussed by Keulegan (1953), Long (1956), Peters & Stoker (1960), Benjamin (1966), Benney (1966) and others (cf. Miles 1979, and references cited therein). We now outline briefly the derivation of (1) for the two-layer configuration shown in figure 1. The basic assumptions are as follows.

(i) The waves are long in comparison with the total fluid depth:

$$k^2(h_1+h_2)^2 \ll 1,$$

where k^{-1} represents a characteristic horizontal wavelength.

(ii) The waves are small, so that if $\bar{\eta}$ denotes a characteristic wave amplitude then

$$\bar{\eta}/(h_1+h_2) \ll 1.$$

(iii) The two effects are in approximate balance:

$$\epsilon = \bar{\eta}/(h_1+h_2) = O[k^2(h_1+h_2)^2] \ll 1.$$

(iv) Viscous effects are weaker than either of these.

(In addition, we assume throughout that the motion is two-dimensional, and that the fluid is incompressible.)

It is consistent with these assumptions to define dimensionless (*) variables as follows

$$z^* = \frac{z}{h_1+h_2}, \quad x^* = \frac{\epsilon^{\frac{1}{2}}x}{h_1+h_2}, \quad t^* = \left(\frac{\epsilon g}{h_1+h_2}\right)^{\frac{1}{2}} t. \tag{8}$$

We also introduce a slow time variable,

$$\tau^* = \epsilon t^*. \tag{9}$$

The interface is defined by

$$\eta = \epsilon(h_1+h_2)\,\eta^*(x^*, t^*, \tau^*; \epsilon); \tag{10a}$$

if the upper surface is free, it is defined by

$$\zeta = h_1 + \epsilon(h_1+h_2)\,\zeta^*(x^*, t^*, \tau^*; \epsilon). \tag{10b}$$

There is a velocity potential in each layer. In the lower fluid, because of Laplace's equation and the boundary condition at $z = -h_2$, the potential has the formal expansion

$$\phi_2 = \phi_0(x^*, t^*, \tau^*; \epsilon) - \tfrac{1}{2}\epsilon^2\left[z^* + \frac{h_2}{h_1+h_2}\right]^2 \frac{\partial^2\phi_0}{\partial(x^*)^2} + O(\epsilon^4).$$

There is a corresponding expansion in the upper fluid. At the interface, the normal velocity and the pressure must be continuous, while the pressure must vanish at the free surface. In addition, both the free surface and the interface satisfy kinematic conditions ($D\zeta/Dt = D\eta/Dt = 0$). Finally, all motion should vanish as $|x| \to \infty$. In order to satisfy these conditions order-by-order in ϵ, it is necessary to expand η^*, ζ^*, and the velocity potentials. Thus, for example

$$\eta^* = \eta_1 + \epsilon\eta_2 + \ldots.$$

At the leading order (infinitely long waves of infinitesimal amplitude), the equations are hyperbolic and linear. An initial disturbance is decomposed into four wave modes:

$$\eta_1 = \sum_{j=1}^{4} f_j\left[\frac{x - c_j t}{(h_1 h_2)^{\frac{1}{2}}}\right], \tag{11}$$

where $[c_j]$ are the four roots in (6). Because these speeds are so different, localized surface and internal waves quickly separate in space.

Weak nonlinear interactions and weak dispersive effects appear on the next scale ($\tau^* = O(1)$), when the expansion is carried to the next order and secular terms are eliminated. There are no nonlinear interactions between modes, because they interact

with each other for too short a time. However, each mode interacts with itself for a long time, and each of the four waves in (11) evolves according to its own KdV equation. Omitting details of the analysis, the dimensional equation for the internal wave mode is

$$c_0^{-1}\frac{\partial \eta}{\partial t}+\frac{\partial \eta}{\partial x}+\frac{3}{2}\left(\frac{1}{h_2}-\frac{1}{h_1}\right)\eta\frac{\partial \eta}{\partial x}+\tfrac{1}{6}h_1h_2\frac{\partial^3\eta}{\partial x^3}=0, \tag{12}$$

where c_0 is given by (6*b*). (Recall that (12) is valid for $\Delta \ll 1$. The generalization to arbitrary Δ is given by Leone, Segur & Hammack (1982) if the upper surface is free, and by Djordjevic & Redekopp (1978) if the upper surface is rigid.) To reduce (12) to (1) let

$$\chi=\frac{x-c_0t}{(h_1h_2)^{\frac{1}{2}}},\quad \tau=\frac{1}{6}\left(\frac{g\Delta}{h_1+h_2}\right)^{\frac{1}{2}}t,\quad f=\frac{3}{2}\left(\frac{1}{h_2}-\frac{1}{h_1}\right)\eta. \tag{13}$$

Then $f(\chi,t)$ satisfies $\qquad f_\tau+6ff_\chi+f_{\chi\chi\chi}=0.$

We now state some of the consequences of KdV theory that may be tested experimentally. More details may be found in Segur (1973), Hammack & Segur (1974, 1978), and elsewhere.

(i) The soliton solution for KdV is

$$f(\chi,\tau)=2\kappa^2\operatorname{sech}^2\{\kappa(\chi-4\kappa^2\tau-\chi_0)\}, \tag{14a}$$

where κ, χ_0 are arbitrary constants. In dimensional terms,

$$\eta=\bar{\eta}\operatorname{sech}^2\{p(x-pvt-x_0)\}, \tag{14b}$$

where

$$p^2=\frac{3(h_1-h_2)\bar{\eta}}{4h_1^2h_2^2},\quad v=\left(\frac{g\Delta h_1h_2}{h_1+h_2}\right)^{\frac{1}{2}}\left[1+\left(\frac{1}{2}\frac{h_1-h_2}{h_1h_2}\right)\bar{\eta}\right]. \tag{14c}$$

These results were given first by Keulegan (1953), except for a misprint. Because $f \geqslant 0$, it follows that an internal soliton always thickens the thin layer. Thus, the soliton raises the interface if $h_1 > h_2$, and lowers it if $h_1 < h_2$.

(ii) In our experiments, $\eta \geqslant 0$ initially. It follows that the internal wave evolves into solitons when $h_1 > h_2$, but not when $h_1 < h_2$.

(iii) The nonlinear term in (12) vanishes if $h_1 = h_2$. We will examine this special case elsewhere (Segur & Hammack 1982). Here we assume $h_1 \neq h_2$.

(iv) Arbitrary initial data that are smooth and localized will evolve into N solitons, ordered by amplitude, followed by a dispersive oscillatory tail. The number of solitons that emerge from $f(\chi,0)$ is the number of zeros of

$$\frac{d^2\psi}{d\chi^2}+f(\chi,0)\psi=0,\quad \psi\to 1 \quad \text{as} \quad \chi\to-\infty. \tag{15}$$

2.2. *The finite-depth equation*

Kubota *et al.* (1978) derived (2) for cases in which the fluid is confined between two rigid walls and the background density distribution is continuous. The derivation we present here differs slightly from theirs because our background density distribution is discontinuous. A more important difference, however, is that our choice of small parameters ($\epsilon \ll 1$) differs from theirs. Both derivations lead to (2), but the scaling of the physical variables is somewhat different. For simplicity, we will use the Boussinesq approximation, and also replace the free surface with a rigid lid.

The assumptions underlying (2) are that:

(i) there is a thin (lower) layer, $\epsilon = h_2/h_1 \ll 1$;

(ii) the characteristic horizontal wavelength is comparable to the depth of the thick layer, $kh_1 = O(1)$;

(iii) wave amplitudes are small, $\bar{\eta}/h_2 \ll 1$;

(iv) these two effects balance, $\bar{\eta}/h_2 = O(\epsilon)$;

(v) viscous effects may be neglected.

Note that the assumption of long waves ($kh_2 \ll 1$) is implied by (i) and (ii). Note further that assumption (iv) is not consistent with corresponding assumption for KdV. Consequently, we may expect the KdV limit of (2) to be somewhat singular.

The following scaling is consistent with the assumptions listed above. In the lower layer, dimensionless (*) variables are

$$x^* = x/h_1, \quad z^* = z/h_2 = z/\epsilon h_1, \quad t^* = \bar{c}t/h_1, \quad \tau = \epsilon t^*. \tag{16a}$$

The wave speed $\bar{c}$ is to be determined. The interface is defined by

$$\eta = \epsilon h_2[\eta_1 + \epsilon\eta_2 + \epsilon^2\eta_3] + O(\epsilon^4). \tag{16b}$$

After satisfying Laplace's equation in the lower fluid and the boundary condition at $z = -h_2$, one finds that the velocity in the lower fluid at the interface may be represented by

$$\left.\begin{aligned} u &= \epsilon\bar{c}\,[u_1(x^*, t^*; \tau, \epsilon) + \epsilon u_2] + O(\epsilon^3), \\ w &= -\epsilon^2\bar{c}\left[\frac{\partial u_1}{\partial x^*} + \epsilon\frac{\partial u_2}{\partial x^*} + \epsilon\eta_1\frac{\partial u_1}{\partial x^*}\right] + O(\epsilon^4). \end{aligned}\right\} \tag{17}$$

Because no further terms will be needed in this expansion in order to derive (2), it will follow that the entire dispersive effect in (2) is due to the upper fluid. It will also turn out that the entire nonlinear effect is due to the lower fluid.

The velocity potential in the upper layer may be written as

$$\phi_1 = \frac{1}{2\pi}\int_{-\infty}^{\infty} \frac{\cosh k(h_1 - z)}{\sinh kh_1}\,\Psi(k, t^*, \tau)\exp ikx\,dk.$$

It is consistent with assumption (ii) to define

$$m = kh_1, \quad x^* = x/h_1, \tag{18}$$

and to rewrite ϕ_1 in terms of these variables. Then if we expand Ψ as

$$\Psi = h_2^2\bar{c}(A_1 + \epsilon A_2 + \ldots), \tag{19}$$

the velocities in the upper fluid at the interface take the form

$$\left.\begin{aligned} U &\sim \frac{i\epsilon^2\bar{c}}{2\pi}\int_{-\infty}^{\infty} (m\coth m)\,(A_1 + \epsilon A_2 + \ldots)\exp imx^*\,dm, \\ W &\sim -\frac{\epsilon^2\bar{c}}{2\pi}\int_{-\infty}^{\infty} m(A_1 + \epsilon A_2 + \ldots)\exp imx^*\,dm, \end{aligned}\right\} \tag{20}$$

There are two kinematic conditions at the interface:

$$\frac{\partial\eta}{\partial t} + u\frac{\partial\eta}{\partial x} = w, \tag{21a}$$

$$(U - u)\frac{\partial\eta}{\partial x} = W - w. \tag{21b}$$

Continuity of pressure at the interface may be written in terms of Bernoulli's law,

$$\frac{\partial \phi_1}{\partial t} + \tfrac{1}{2}(U^2 + W^2) - \frac{\partial \phi_2}{\partial t} - \tfrac{1}{2}(u^2 + w^2) - g\Delta\eta = \text{const.}, \tag{21c}$$

once we have made the Boussinesq approximation. Because (21*c*) is valid along the interface, its tangential derivative vanishes there. Substituting (17) and (20) into these conditions, one finds that non-trivial solutions exist at leading order if

$$\bar{c}^2 = g\Delta h_2, \tag{22}$$

as anticipated by (7). (A major difference between this derivation and one following Kubota *et al.* (1978) is that their leading-order wave speed satisfies

$$\bar{c}^2 = g\Delta h_2(1-\epsilon).$$

Thus, they retain a term at leading order that we regard as a higher-order effect. This difference in ordering persists at higher orders in the expansion.) In the present derivation, the solution of the leading-order equations is

$$\left.\begin{aligned} \eta_1(x^*, t^*, \tau) &= f(r,\tau) + g(l,\tau), \\ u_1(x^*, t^*, \tau) &= f(r,\tau) - g(l,\tau), \\ A_1(x^*, t^*, \tau) &= i\hat{f}(m,\tau)\exp(-imt^*) - i\hat{g}(m,\tau)\exp imt^*, \end{aligned}\right\} \tag{23}$$

where

$$r = x^* - t^*, \quad l = x^* + t^*,$$

(^) denotes the Fourier transform (assumed to exist), and we have used the boundary condition that all motion ceases as $|x| \to \infty$.

Secular terms arise at the next order unless the right-going waves satisfy

$$2\frac{\partial f}{\partial \tau} + 3f\frac{\partial f}{\partial r} - \frac{\partial}{\partial r}\frac{1}{2\pi}\int (m \coth m)\hat{f}(m,\tau)\exp imr\, dm = 0, \tag{24a}$$

and the left-going waves satisfy a similar equation. This nonlinear evolution equation has several representations. Another is

$$2\frac{\partial f}{\partial \tau} + 3f\frac{\partial f}{\partial r} - \frac{1}{2}\frac{\partial^2}{\partial r^2}\int f(y,\tau)\coth \tfrac{1}{2}\pi(r-y)\, dy = 0. \tag{24b}$$

which may be scaled to (2). In dimensional variables

$$(\bar{c})^{-1}\frac{\partial \eta}{\partial t} + \frac{\partial \eta}{\partial x} + \frac{3}{2}\frac{\eta}{h_2}\frac{\partial \eta}{\partial x} - \frac{h_2}{4h_1}\frac{\partial^2}{\partial x^2}\int \coth\left(\tfrac{1}{2}\pi\frac{x-z}{h_1}\right)\eta\left(\frac{z}{h_1}\right)dz = 0, \tag{25}$$

where $\bar{c}$ is defined by (22).

In this derivation we have assumed that all functions vanish as $|x| \to \infty$. Periodic boundary conditions are more natural in many problems, such as when the waves are generated by the periodic motion of the tides. In this case it is necessary only to replace the Fourier integrals with Fourier sums. The analogue of (24) on $(-\pi, \pi)$ with periodic boundary conditions is

$$2\frac{\partial f}{\partial \tau} + 3f\frac{\partial f}{\partial r} - \frac{\partial}{\partial r}\frac{1}{2\pi}\sum_{-\infty}^{\infty} n \coth n\hat{f}_n(\tau)\exp inr = 0, \tag{26a}$$

where $[\hat{f}_n]$ are the coefficients of the Fourier-series representation of f. The sum in (26a) can be written as a convolution integral, with a kernel involving elliptic functions. The derivation of (26a) also requires

$$\hat{f}_0(\tau) = \int_{-\pi}^{\pi} f(r,\tau)\,dr = 0, \tag{26b}$$

which amounts to a normalization. The analysis of (26) is quite similar to that of (24), as discussed by Ablowitz *et al.* (1982).

Based on the work of Joseph & Egri (1978), Chen & Lee (1979), Satsuma, Ablowitz & Kodama (1979), and Kodama, Satsuma & Ablowitz (1981), we may assert that (24) is completely integrable, and that its solutions are qualitatively similar to those of the KdV equation. In particular, a soliton solution of (24) is

$$\tfrac{3}{2}f = \frac{\lambda \sin\lambda}{\cos\lambda + \cosh\lambda[r + \frac{1}{2}\tau\lambda\cot\lambda + r_0]}, \tag{27a}$$

where (λ, r_0) are arbitrary parameters except that $0 \leqslant \lambda < \pi$. In dimensional terms

$$\frac{\eta}{h_2} = \frac{\frac{2}{3}(h_2/h_1)\,\lambda\sin\lambda}{\cos\lambda + \cosh\theta} \tag{27b}$$

$$\theta = \lambda\frac{(x+x_0)}{h_1} - \frac{\lambda\bar{c}t}{h_1}\left[1 - \frac{1}{2}\frac{h_2}{h_1}\lambda\cot\lambda\right]. \tag{27c}$$

This reduces to a KdV soliton in the limit $\lambda \to 0$, h_2/h_1 fixed.

In order to carry this expansion to higher order, it is convenient to consider only right-going waves, so that $g(l,\tau) \equiv 0$ in (23). Then at second order

$$\left.\begin{aligned} \eta_2(r,\tau) &= f_2 \\ u_2 &= f_2 - \tfrac{1}{4}f^2 + \frac{1}{2}\frac{\partial}{\partial r}T[f], \\ \frac{i}{2\pi}\int A_2 \exp imx^*\,dm &= -f_2 - \tfrac{3}{4}f^2 - \frac{1}{2}\frac{\partial}{\partial r}T[f]. \end{aligned}\right\} \tag{28}$$

At second order $f_2(r,\tau)$ is free, but secular terms arise at third order unless

$$L[f_2] = \tfrac{1}{2}f\frac{\partial f}{\partial \tau} + \frac{3}{2}\frac{\partial^2}{\partial r\partial\tau}T[f] + \frac{1}{2}\frac{\partial}{\partial r}(f^3) - \frac{\partial}{\partial r}\left(f\frac{\partial}{\partial r}T[f]\right) - \frac{1}{3}\frac{\partial^3 f}{\partial r^3}, \tag{29}$$

where f is a solution of (24), and

$$L[v] = 2\frac{\partial v}{\partial \tau} + 3\frac{\partial}{\partial r}(fv) + \frac{\partial^2}{\partial r^2}T[v].$$

Because $L(v)$ is the linearization of (24), one finds easily that

$$L\left[\frac{\partial f}{\partial r}\right] = L\left[\frac{\partial f}{\partial \tau}\right] = 0, \tag{30a}$$

$$L\left[\tau\frac{\partial f}{\partial r}\right] = 2\frac{\partial f}{\partial r}, \tag{30b}$$

$$L[f] = \frac{3}{2}\frac{\partial}{\partial r}(f^2). \tag{30c}$$

We now seek specifically the second-order correction to a soliton (27) so that

$$\frac{\partial f}{\partial \tau} \sim -(c_1+\epsilon c_2)\frac{\partial f}{\partial r}, \quad \frac{\partial f_2}{\partial \tau} \sim -c_1\frac{\partial f_2}{\partial r},$$

and c_2 is to be determined. Moreover,

$$\frac{\partial}{\partial r}T[f]+\tfrac{3}{2}f^2-2c_1 f \sim 0,$$

$$\frac{\partial^2 f}{\partial r^2} = \lambda^2 f+9c_1 f^2-\tfrac{9}{2}f^3.$$

In this case, (29) reduces to

$$L[f_2] = \frac{\partial}{\partial r}\{(2c_2-3c_1^2-\tfrac{1}{3}\lambda^2)f-3c_1 f^2+\tfrac{7}{2}f^3\}. \tag{31}$$

From (30*a*), this equation has no unique solution. From (30*b*), we must choose

$$2c_2 = 3c_1^2+\tfrac{1}{3}\lambda^2, \tag{32}$$

in order to avoid unbounded growth in f_2. Thus the dimensional speed of a soliton to this order is

$$C \sim \bar{c}\,[1-\tfrac{1}{2}\epsilon\lambda\cot\lambda+\tfrac{1}{2}\epsilon^2\lambda^2(\tfrac{3}{4}\cot^2\lambda+\tfrac{1}{3})], \tag{33}$$

where $\epsilon = h_2/h_1$, and λ is the parameter for the soliton.

In the small-amplitude limit, $\lambda \to 0$ and (33) reduces to the expansion of (6*b*) for small ϵ. At the other extreme, if $\lambda \to \pi$ then to this order of approximation,

$$C \sim \bar{c}\left(1-\frac{\epsilon\pi}{\pi-\lambda}\right)^{-\frac{1}{2}}.$$

Clearly

$$\lambda < \pi(1-\epsilon) \tag{34}$$

is necessary for the validity of (33) as an asymptotic expansion. It is probably not sufficient. Joseph & Adams (1981) also carried this expansion to second order in a related problem. They suggest that their expansion is valid only if $C < 1{\cdot}4c_*$, where c_* corresponds to C_0, defined by (6*b*). In this problem, their cutoff corresponds to about

$$\lambda < \pi(1-2\epsilon).$$

However, they give no clear criterion for this choice.

We now return to (31). Let $v(r)$ denote a particular solution of

$$L[v] = \frac{\partial}{\partial r}\{f^3\}. \tag{35}$$

We have found no analytic expression for $v(r)$, but a numerical procedure to solve (35) approximately is outlined in the appendix. A solution of (31), corresponding to $f[r-(c_1+\epsilon c_2)\tau;\,\lambda]$ is

$$f_2 = -2c_1 f+\tfrac{7}{2}v, \tag{36}$$

or

$$\eta \sim \epsilon h_2[(1-2\epsilon c_1)f+\tfrac{7}{2}\epsilon v].$$

This is the expression that we will compare with our data in § 3.

In the experiments of Koop & Butler (1981), the dimensionless density difference $\Delta = 0{\cdot}367$, and the Boussinesq approximation is invalid. However, the analysis for arbitrary Δ follows nearly identical lines, and we may simply state the main results.

With the thin layer on the bottom and a free surface on top, the leading-order wave speed is still given by (22). The evolution equation becomes

$$2\frac{\partial \tilde{f}}{\partial \tau}+3\tilde{f}\frac{\partial \tilde{f}}{\partial r}+(1-\Delta)\frac{\partial^2}{\partial r^2}T[\tilde{f}]=0, \tag{37}$$

instead of (24). For fixed λ, the relation between a soliton with $\Delta \neq 0$, $(\tilde{f}, \tilde{c}_1)$ and the earlier results (f, c_1) is

$$\tilde{c}_1(\lambda;\Delta)=(1-\Delta)c_1(\lambda), \quad \tilde{f}=(1-\Delta)f(r-\tilde{c}_1\tau;\lambda). \tag{38}$$

The evolution equation for $\tilde{f}_2$ is somewhat complicated, but if $\tilde{f}$ is a soliton and $\tilde{f}_2$ is a permanent wave travelling with the same speed, then

$$\begin{aligned}\tilde{L}[\tilde{f}_2] &\equiv \frac{\partial}{\partial r}\left\{-2\tilde{c}_1\tilde{f}_2+3\tilde{f}\tilde{f}_2+(1-\Delta)\frac{\partial}{\partial r}T[\tilde{f}_2]\right\}\\ &=\frac{\partial}{\partial r}\left\{\left[2\tilde{c}_2-3\tilde{c}_1^2-\tfrac{1}{3}\lambda^2+\Delta(1-\Delta)\left(\frac{\lambda}{\sin\lambda}\right)^2\right]\tilde{f}\right.\\ &\qquad\left.-\frac{3\tilde{c}}{(1-\Delta)^2}\tilde{f}^2+\frac{7-17\Delta+13\Delta^2}{2(1-\Delta)^2}\tilde{f}^3-\frac{3\Delta}{2}\frac{\partial}{\partial r}T[\tilde{f}]\right\}.\end{aligned} \tag{39}$$

The result is

$$\left.\begin{aligned}2\tilde{c}_2 &= 3\tilde{c}_1^2+\tfrac{1}{3}\lambda^2-\Delta(1-\Delta)\left(\frac{\lambda}{\sin\lambda}\right)^2,\\ \tilde{f}_2 &= -2\tilde{c}_1\frac{(1+\Delta-\Delta^2)}{(1-\Delta)^2}\tilde{f}-\frac{3\Delta}{2(1-\Delta)}\tilde{f}^2+[2(1-\Delta)^2+\tfrac{3}{2}]v,\end{aligned}\right\} \tag{40}$$

where $(\tilde{f}, \tilde{c}_1)$ satisfy (38), and v satisfies (35). Let $\bar{\eta}$ denote the maximum displacement of the interface. Then it follows from (40) that

$$\begin{aligned}\frac{h_1\bar{\eta}}{(1-\Delta)h_2^2} &= \frac{\frac{2}{3}\lambda\sin\lambda}{1+\cos\lambda}\left[1+\epsilon\lambda\cot\lambda\,\frac{1+\Delta-\Delta^2}{(1-\Delta)^2}-\frac{\epsilon\Delta\lambda\sin\lambda}{1+\cos\lambda}\right]\\ &\qquad+\epsilon\left[2(1-\Delta)+\frac{3}{2(1-\Delta)}\right]V_{\max}+O(\epsilon^2).\end{aligned} \tag{41}$$

Koop & Butler (1981) define an integral length scale by

$$\bar{\eta}\Lambda \equiv \int_0^\infty \eta\, dx. \tag{42}$$

It follows from the results above that

$$\frac{\bar{\eta}\Lambda}{h_2^2}=\frac{2\lambda}{3}(1-\Delta)+\tfrac{2}{3}\epsilon\lambda^2\cot\lambda+\epsilon(2(1-\Delta)^2+\tfrac{3}{2})\,I+O(\epsilon^2), \tag{43}$$

where

$$I=\int_0^\infty v(r)\,dr,$$

and must be found numerically.

3. Comparison with experiments

A series of experiments was performed in which long internal waves were generated by the vertical uplift of a rectangular piston at one end of a wave tank, as shown schematically in figure 1. The tank was 30 m long, 60 cm deep, and 39·4 cm wide. The piston was 61 cm long and spanned the tank width. The time-displacement history of

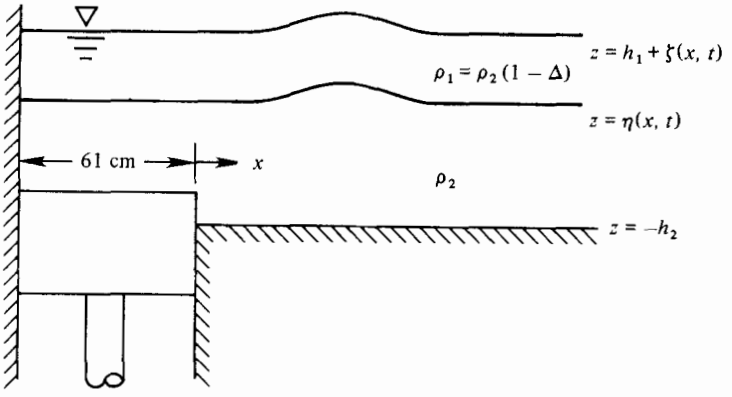

FIGURE 1. Piston moves up into a two-layer system, generating waves both at the free surface (ζ) and at the interface (η).

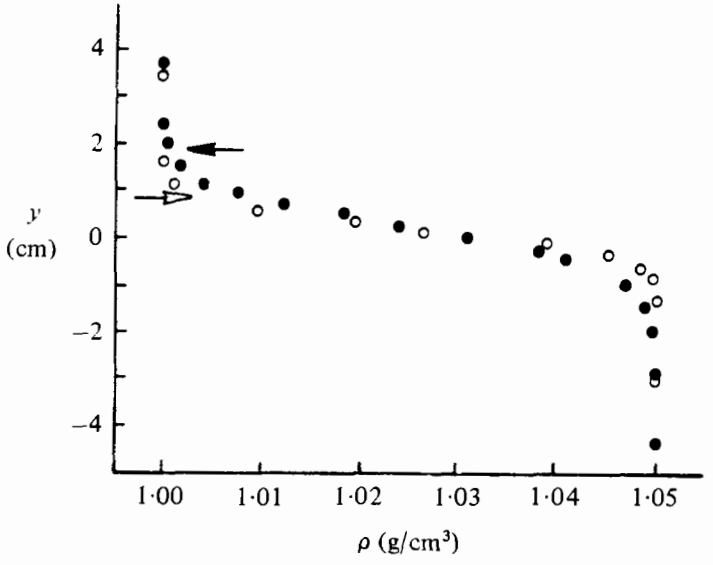

FIGURE 2. Typical density stratifications before (○) and after (●) a set of experiments. Arrows indicate the position of the dye interface.

the piston was controlled by electrohydraulic-servo system, so that repeatable motions were easily obtained. Both the tank and wavemaker have been described in detail by Hammack (1972).

The stratified fluid used in these experiments consisted of a layer of fresh water overlying a layer of brine with $h_1 = 45$ cm, $h_2 = 5$ cm and $\Delta = 0{\cdot}048$. Actual density stratifications were measured using a conductivity probe before, during, and after a set of experiments. In all cases the initial thickness of the interfacial region (pycnocline) was about 1 cm; experiments were terminated when the pycnocline thickness reached 2 cm. Typical beginning and ending stratifications near the pycnocline are shown in figure 2. Because the density varied continuously with depth in the experiments, linear

theory would predict an infinite set of internal wave modes. However, we are primarily interested in the lowest internal wave mode, for which the two-layer model discussed in §2 is applicable.

Detailed discussions of the tank-filling procedures and stratification properties are given by Hammack (1980), where it is demonstrated that the growth of the interfacial thickness was dominated by molecular diffusion. Hence, the shear layers produced by these long waves at the pycnocline were laminar and did not cause appreciable mixing.

Rapid uplift of the rectangular piston generated both surface and internal waves. Both initial waves were rectangular in shape, with a length of 122 cm (twice the piston length since the tank end wall adjacent to the piston acts as a plane of symmetry in linear, inviscid theory). The maximum amplitude of the surface wave was one-half the piston uplift, while the internal-wave amplitude was further attentuated by the ratio $h_1/(h_1+h_2)$. (A detailed analysis and discussion of the generation process is given by Hammack 1980.) The faster surface wave separated quickly from the internal wave so that there was effectively no interaction. In order to prevent the surface wave from returning to the internal wave region, a vertical plate, located 18·8 m from the piston, was lowered carefully into the water after the passage of the surface wave. In addition to trapping the surface wave, the plate effectively lengthened the test section for the internal wave, since this wave eventually reflected off the plate and propagated back through the test section.

Internal wave measurements were obtained using a laser-optics-detector system described by Hammack (1980). Briefly, the light beam of a laser was converted to a uniform-width light sheet that was directed across the glass-walled tank. With the quiescent interface intercepting the light sheet and the brine dyed blue, subsequent displacements of the interface varied the amount of light traversing the tank cross-section. (The dye interface remained sharp and distinct throughout a set of experiments. It was always located near the top of the salinity interface, as shown in figure 2.) The transmitted light was focused onto a photodetector, whose output voltage was recorded. The system was calibrated before each experiment to determine the (non-linear) correlation between output voltage of the photodetector and the vertical displacement of the interface. Only one gauge was available; hence the same experiment was repeated in order to measure time histories of the interfacial displacement at various positions along the tank. Both the repeatability of the piston motion and the quiescent conditions prior to an experiment were carefully monitored and assured for all reported data. The small changes in the background stratification between experiments led to slight changes in the phase speed of the internal waves.

Figure 3 shows the evolution of the internal wave, as measured at seven downstream locations in the tank. The co-ordinate system in figure 3 moves with the linearized wave speed c_0, and reverses the sense of direction of the wave. Thus the front of these waves is to the left in each record. Moreover, we have omitted the weak train of oscillatory waves that follows the dominant waves that are shown. The first five measurements were recorded ahead of the plate at $x/(h_1h_2)^{\frac{1}{2}} = 125$.

For this experiment the piston uplift was 2 cm, so we may take $k^{-1} = 122$ cm, and $\bar{\eta} = 1$ cm, corresponding to the dominant length scale and maximum amplitude of the initial wave. Hence, $k^2(h_1+h_2)^2 \sim 0{\cdot}16$, $\bar{\eta}/(h_1+h_2) \sim 0{\cdot}02$, and we may apply KdV theory at least provisionally. Using either the first or second wave record as the potential in (15), one finds that according to KdV theory, this wave should evolve into

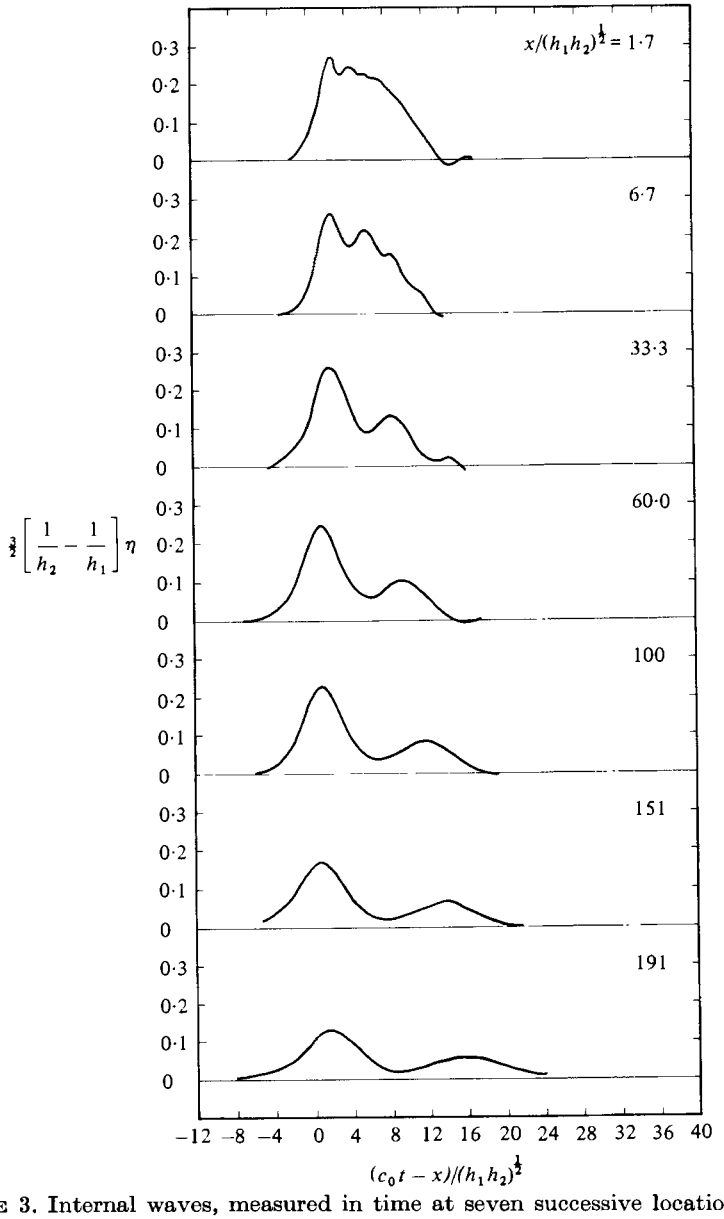

FIGURE 3. Internal waves, measured in time at seven successive locations. $h_1 = 45$ cm, $h_2 = 5$ cm, $\Delta = 0{\cdot}048$. A vertical plate inserted during the experiment at $x/(h_1h_2)^{\frac{1}{2}} = 125$ reflected the wave train back into the test section for the last two measurements.

two solitons, followed by a weak oscillatory wave train. Certainly this prediction is in qualitative agreement with the wave records shown in figure 3.

A more rigorous test of KdV theory is shown in figure 4, where we have plotted the lead wave from each of the last five records on a single graph. According to (14), the data from all of these wave records should fall on a single curve once the peak amplitude at each station is known. The agreement in figure 4 between the predicted wave shape and all of these data is so good that we conclude that these are (locally) KdV solitons.

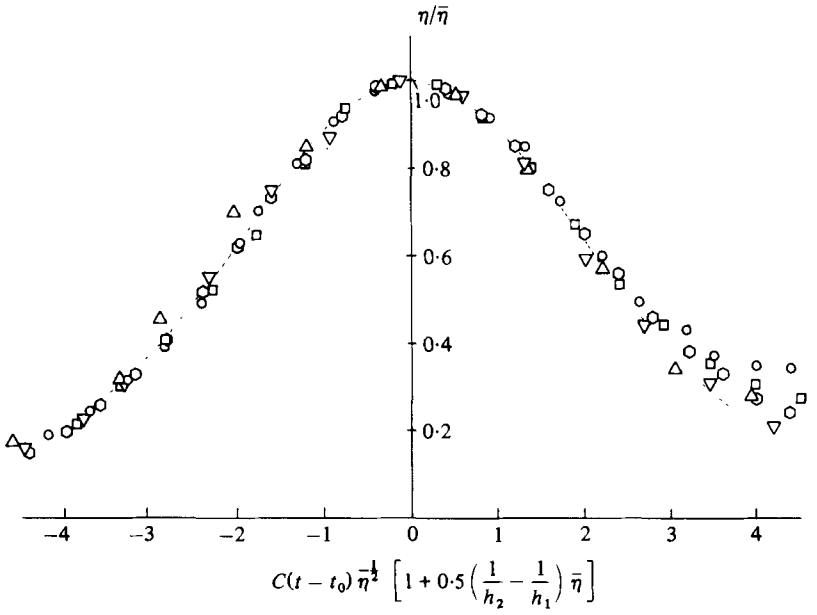

FIGURE 4. Comparison of the lead waves in the last five measurements in Figure 3 with the shape of a KdV soliton, according to (14). $C^2 = [3g\Delta(h_1-h_2)/4(h_1h_2)^3] \times 8063$. ○, $x/(h_1h_2)^{\frac{1}{2}} = 33{\cdot}3$; □, 60; ⬡, 100; △, 151; ▽, 191; - - - -, KdV theory.

The major discrepancies between the predicted and observed wave shapes occur: (i) at the rear (i.e. right) of each wave, where the influence of the trailing soliton becomes important; and (ii) in the data at $x/(h_1h_2)^{\frac{1}{2}} = 151$, just downstream of the reflecting plate, where the incident and reflected waves from this plate apparently are still superposed.

The amplitude of the soliton is slowly decaying at its propagates down the tank, presumably due to viscosity, but this decay is sufficiently slow that the wave continually readjusts its shape as it decays so that it is locally a KdV soliton. On the basis of a much larger set of experiments, Hammack & Segur (1974) found that this same description (locally KdV solitons, slowly attenuated by viscosity) also applies to the corresponding long surface waves. Leone, Segur & Hammack (1981) discuss the viscous decay of these waves.

Based on the remarkably good agreement in figure 4, and the fact that initially $k^2(h_1+h_2)^2$ exceeds $\bar{\eta}/(h_1+h_2)$ by a factor of about 10, it is tempting to conclude that the KdV equation has a fairly large range of validity. This conclusion may well be correct, but it is not necessarily implied by figure 4. While $k^2(h_1+h_2)^2 \sim 0{\cdot}16$ may describe the initial data, the evolving solitons have characteristic wavelengths that are much longer, so that the required balance is achieved for the solitons. The stronger conclusion applies only if the equation predicts correctly from the initial data the wavelengths of the solitons that emerge.

KdV theory predicts that all solitons should move somewhat faster than c_0, the linear long-wave speed, and therefore should move slowly to the left in figure 3. The larger, faster soliton does move somewhat to the left until the last station, but the smaller soliton clearly is moving slowly to the right. Thus, the observed speeds of the

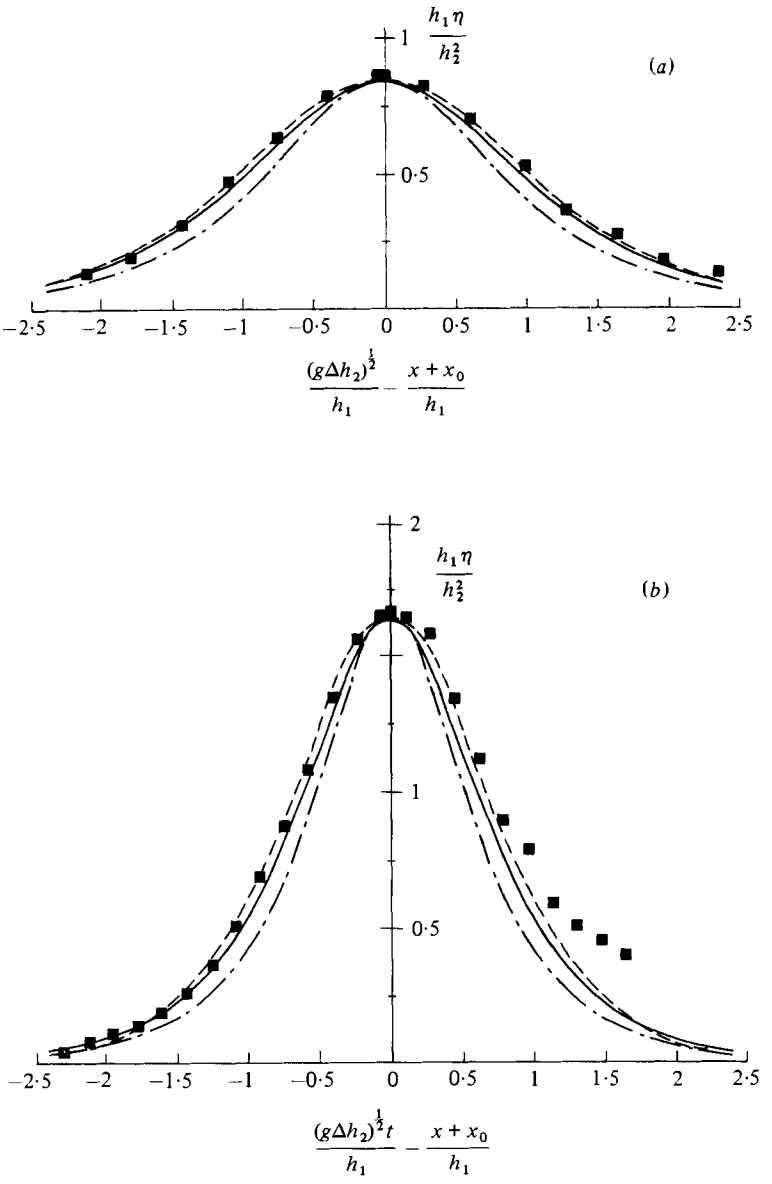

FIGURE 5. Comparison of two of the measured lead waves in figure 3 with three theoretical shapes, each having the same peak amplitude as that measured. (*a*) $x/(h_1h_2)^{\frac{1}{2}} = 191$; (*b*) 60. — — —, KdV (14); — · —, first-order finite-depth (27); ——, second-order finite-depth, (36); ■, measured.

solitons are slower than those predicted by KdV theory, and sometimes even slower than c_0. This discrepancy was observed for surface solitons as well (Hammack & Segur 1974). For internal waves, we note that the predicted wave speeds could be reduced by generalizing the theory to include the influence either of the finite thickness of the pycnocline or of viscosity.

Next, we consider the finite-depth equation, (24). There seems to be no simple way to compare all of the data on one figure for (24), but in figure 5 we show the lead waves measured at two representative points, $x/(h_1h_2)^{\frac{1}{2}} = 60$ and 191. Figure 5 also shows the

wave shapes predicted by KdV theory (14), by the first-order finite-depth theory (27), and by the second-order finite-depth theory (36). In all cases, the free parameter available in the theory (e.g. λ in (27)) was chosen to match the peak amplitude of the measured wave. It is apparent that while all of these theoretical predictions are reasonably accurate, first-order finite-depth theory is noticeably less accurate than KdV theory. The discrepancy is apparent even at $x/(h_1 h_2)^{\frac{1}{2}} = 191$, where $h_2/h_1 = \frac{1}{9}$, $\overline{\eta}/h_2 \sim 0{\cdot}094$, and one might expect (27) to be quite accurate.

Figure 5 supports the claim that the range of validity of the asymptotic expansion that leads to the finite-depth equation is small. In figure 5(*a*), where the peak wave amplitude is rather small, the second-order finite-depth theory predicts the measured data about as well as does KdV theory. The peak amplitude in figure 5(*b*) is about twice that in figure 5(*a*), and here even the second-order theory is beginning to fail. Presumably, third-order corrections now have become important.

As an independent test of the hypothesis that the range of validity of (24) is rather small in a practical sense, we analyse next the experimental results of Koop & Butler (1981). Figure 6 shows the relation between soliton amplitude (41) and integral length scale (43), corresponding to figures 10 and 12 of Koop & Butler. The first-order curve is obtained by letting $\epsilon \to 0$ in (41) and (43). Higher-order corrections depend on $\epsilon = h_2/h_1$ and on $\Delta = (1-\rho_1/\rho_2)$, and we show in figures 6(*a*, *b*) two second-order curves, corresponding to the two configurations of Koop & Butler. Note that both second-order curves terminate at finite values of $\overline{\eta}h_1/(1-\Delta)h_2^2$. This termination occurs because $\overline{\eta}h_1/(1-\Delta)h_2^2$ has a maximum in (41) as a function of λ, signalling a breakdown of the asymptotic series. This breakdown occurs earlier than that in (34).

A comparison of the first-order theory, second-order theories, and the data in figure 6 reveals the following facts.

(i) In figure 6(*a*) ($\epsilon = 0{\cdot}197$, corresponding to figure 10 of Koop & Butler) there are no data with amplitudes sufficiently small that the first- and second-order theories coincide. In this sense, the first-order theory by itself must be considered inadequate to represent these data.

(ii) For $\epsilon = 0{\cdot}197$, the second-order theory predicts the data quite well within its range of validity. However, a significant portion of the data lies outside the range of validity of the theory.

(iii) In figure 6(*b*) ($\epsilon = 0{\cdot}029$) the first- and second-order theories are in close agreement over the entire range of validity of the theory. Both predict wave amplitudes somewhat larger than those observed, especially for the longer (and therefore, smaller) waves. This effect is less pronounced but also evident in figure 6(*a*). Koop & Butler noted that even the KdV equation has this problem for very long waves; they argued that it is a viscous effect.

(iv) For $\epsilon = 0{\cdot}029$, *most* of the data lies beyond the range of validity of the theory. There is no obvious physical mechanism, such as wave breaking, that precipitates the breakdown of the theory.

Finally, we summarize our major conclusions.

(i) Both (1) and (2) are valid (formally) asymptotic equations that govern the slow evolution of long internal waves of small amplitude that propagate in one direction in an inviscid fluid. However, the meaning of 'long' is different in the two theories, which describe perturbations to two different wave equations, with two different speeds.

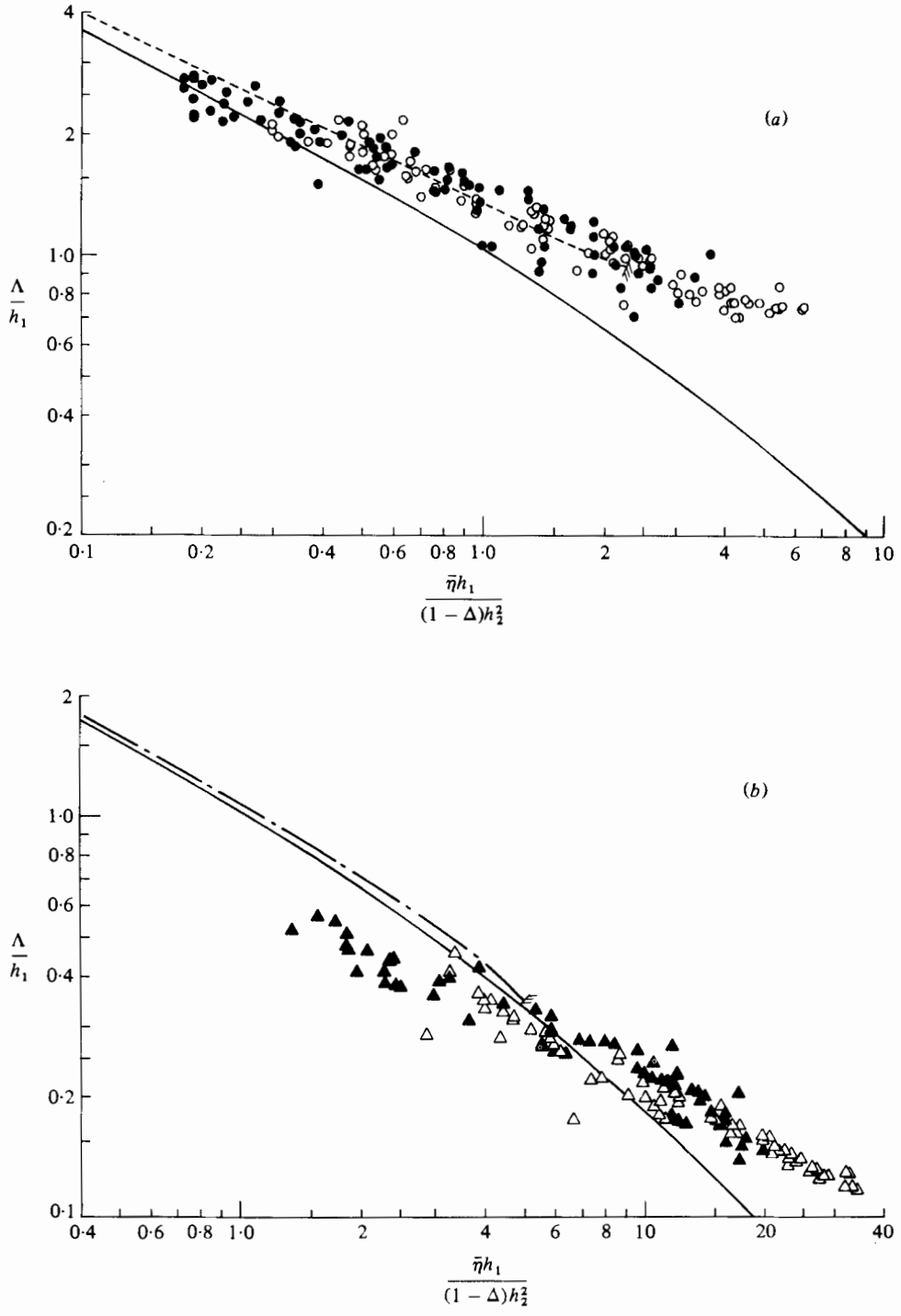

FIGURE 6. Relation between integral wavelength (43) and peak amplitude (41) for internal solitary waves in a fluid of finite depth. (*a*) $\epsilon = h_2/h_1 = 0{\cdot}197$, $\Delta = 1-\rho_1/\rho_2 = 0{\cdot}367$; ——, first-order finite-depth theory, with $\epsilon = 0$ in (41) and (43); – – – –, second-order finite-depth theory; ○, incident waves measured by Koop & Butler (1981); ●, measured reflected waves. (*b*) $\epsilon = 0{\cdot}029$, $\Delta = 0{\cdot}367$; ——, first-order finite-depth theory; —·—, second-order finite-depth theory; △, measured incident waves; ▲, measured reflected waves.

(ii) The KdV equation (1) seems to have a relatively large range of validity, and has practical predictive value even when its assumptions are satisfied only marginally.

(iii) The finite-depth equation (2) by itself has such a small range of validity that it has been difficult even to find it experimentally.

(iv) The asymptotic expansion that generates (2) has a larger range of validity, but it is also quite limited. In particular, there is a range of wave amplitudes for which the long waves in question are too small to break, but too large to be predicted by the finite-depth theory, of any order.

The experiments on which figures 1–5 were based were performed at the W. M. Keck Laboratory of Hydraulics and Water Resources at the California Institute of Technology during 1973–74. We acknowledge our debt to Elton Daly and his staff who assisted in the design, construction, and maintenance of experimental facilities, to Martin Kruskal for several helpful conversations regarding the derivation of (24), and to Gary Koop for providing us with the data in figure 6 prior to its publication. Financial support was provided in part by the Office of Naval Research, Fluid Dynamics Division and the National Science Foundation. The second author would like to acknowledge the first author, whose creative interpretation of the data and persistence made this paper possible.

Appendix

For permanent localized waves, (35) is equivalent to

$$L_1[v] \equiv (3f - 2c_1)v + \frac{\partial}{\partial r} T[v] = f^3, \tag{A 1}$$

where $f(r;\lambda)$ denotes a soliton with speed $c_1(\lambda)$. A Galerkin procedure may be used to solve (A 1) approximately. Here (A 1) is replaced by a finite set of equations of the form

$$(L_1[v], \phi_n) = (f^3, \phi_n) \quad (n = 0, \ldots, N), \tag{A 2}$$

where $(a, b) = \int ab\, dr$, and $[\phi_n(r)]$ denotes a set of basis functions of a finite-dimensional space of functions on $-\infty < r < \infty$. We have chosen to use

$$\phi_n(r) = (n!)^{-\frac{1}{2}} He_n(r) \exp(-\tfrac{1}{4}r^2), \tag{A 3}$$

where $He_n(r)$ are Hermite polynomials (notation as in Abramowitz & Stegun 1964). These basis functions could be generalized by including a scaling factor ($r \to \alpha r$), but (A 3) was adequate for our purposes. These functions are orthogonal, and their Gaussian decay mimics the localized nature of the soliton. Therefore, if the soliton width matches roughly the width of the Gaussian filter then very few basis functions are required to represent a soliton to a high degree of accuracy.

A soliton is an even function in its argument. Both $L_1[\ ]$ and the right-hand side of (A 1) are also even, and (A 1) has a solution that is even. Therefore, we use only the even basis functions, $\phi_{2n}(r)$, in (A 2). This choice excludes the solution of the homogeneous problem in (30a), and seems to make (A 2) well-posed. Certainly it is computationally stable if only $[\phi_{2n}]$ are used.

After expanding

$$f(r) = \sum_0^N \hat{f}_{2n}\phi_{2n}(r), \quad v(r) = \sum_0^N \hat{v}_{2n}\phi_{2n}(r), \tag{A 4}$$

(A 2) reduces to a set of linear algebraic equations for $[\hat{v}_{2n}]$, the coefficients of which are obtained by evaluating certain integrals. The only delicate question is to decide what accuracy is achieved with a certain N in (A 4). We used three main tests of numerical accuracy.

(i) For a soliton $f(r, \lambda)$ we have that

$$2c_1(\lambda) = \frac{\frac{3}{2}(f^2, f) + (\partial T[f]/\partial r, f)}{(f, f)}. \tag{A 5}$$

Using (A 4) in (A 5) yields a sequence $2c_1(\lambda; N)$, which may be compared to the exact result $2c_1(\lambda) = -\cot\lambda$. With $N = 7$, the error in $2c_1$ remained below 10^{-2} for

$$\tfrac{1}{10}\pi \leqslant \lambda \leqslant \tfrac{1}{2}\pi,$$

increased to about 0·2 for $\lambda = \frac{2}{3}\pi$, and continued to increase for larger values of λ. Regardless of how well it approximates $-\lambda\cot\lambda$, the solution of (A 5) is the appropriate value of $2c_1$ for the truncated problem, and it was used in $L_1[\ ]$.

(ii) It follows from (30*c*) that an exact solution of

$$L_1[w] = f^2 \tag{A 6}$$

is $w = \frac{2}{3}f$. Let $[\hat{w}_{2n}]$ denote the coefficients obtained by solving (A 6) approximately, and measure the error in this approximate solution by

$$e_2 = \max_{0 \leqslant n \leqslant N} |\hat{w}_{2n} - \tfrac{2}{3}\hat{f}_{2n}|/|\hat{f}_0|. \tag{A 7}$$

For $N = 7$, we find $e_2 < 10^{-2}$ for $\frac{1}{4}\pi \leqslant \lambda \leqslant \frac{1}{2}\pi$, and $e_2 < 6 \times 10^{-2}$ for $\frac{1}{10}\pi \leqslant \lambda \leqslant \frac{3}{4}\pi$.

(iii) Truncation of the series at N requires that the first few terms dominate the series. Let $\hat{v}_{2n}$ denote the coefficients in the solution of (A 2), and define

$$e_3 = \max\{|\hat{v}_{12}|, |\hat{v}_{14}|\}/|\hat{v}_0|. \tag{A 8}$$

For $N = 7$, $e_3 < 2 \times 10^{-2}$ if $\frac{1}{4}\pi \leqslant \lambda \leqslant \frac{1}{2}\pi$, and $e_3 < 7 \times 10^{-2}$ if $\frac{1}{10}\pi \leqslant \lambda \leqslant \frac{3}{4}\pi$.

REFERENCES

Ablowitz, M. J., Fokas, A. S., Satsuma, J. & Segur, H. 1982 On the periodic intermediate long wave equation. *J. Phys.* A: *Math. & Gen.* (to appear).

Abramowitz, M. & Stegun, L. A. 1964 *Handbook of Mathematical Functions.* N.B.S., Washington, D.C.

Benjamin, T. B. 1966 *J. Fluid Mech.* **25**, 241.

Benjamin, T. B. 1967 *J. Fluid Mech.* **29**, 559.

Benney, D. J. 1966 *J. Math. & Phys.* **45**, 52.

Chen, H. H. & Lee, Y. C. 1979 *Phys. Rev. Lett.* **43**, 264.

Djordjevic, V. D. & Redekopp, L. G. 1978 *J. Phys. Oceanog.* **8**, 1016.

Hammack, J. L. 1972 Tsunamis - a model of their generation and propagation. *W. M. Keck Lab., Caltech Rep.* KH-R-28.

Hammack, J. L. 1980 *J. Phys. Oceanog.* **10**, 1455.

Hammack, J. L. & Segur, H. 1974 *J. Fluid Mech.* **65**, 289.

Hammack, J. L. & Segur, H. 1978 *J. Fluid Mech.* **84**, 337.

Joseph, R. I. 1977 *J. Phys.* A, *Math. & Gen.* **10**, L225.

Joseph, R. I. & Adams, R. C. 1981 *Phys. Fluids* **24**, 15.

Joseph, R. I. & Egri, R. 1978 *J. Phys.* A, *Math. & Gen.* **11**, L97.

Keulegan, G. H. 1953 *J. Res. Nat. Bur. Stand.* **51**, 133.

KODAMA, Y., SATSUMA, J. & ABLOWITZ, M. J. 1981 *Phys. Rev. Lett.* **46**, 687.

KOOP, C. G. & BUTLER, G. 1981 *J. Fluid Mech.* **112**, 225.

KORTEWEG, D. J. & DE VRIES, G. 1895 *Phil. Mag.* **39**, ser. 5, 422.

KUBOTA, T., KO, D. R. S. & DOBBS, L. 1978 *A.I.A.A. J. Hydronaut.* **12**, 157.

LAMB, H. 1932 *Hydrodynamics*. Dover.

LEONE, C., SEGUR, H. & HAMMACK, J. L. 1982 Viscous decay of long internal solitary waves, Preprint.

LONG, R. R. 1956 *Tellus* **8**, 460.

MILES, J. W. 1979 *Tellus* **31**, 456.

ONO, H. 1975 *J. Phys. Soc. Japan* **39**, 1082.

OSBORNE, A. R. & BURCH, T. L. 1980 *Science*, **208**, 451.

PETERS, A. S. & STOKER, J. J. 1960 *Commun. Pure Appl. Math.* **13**, 115.

SATSUMA, J., ABLOWITZ, M. J. & KODAMA, Y. 1979 *Phys. Lett.* **73A**, 283.

SEGUR, H. 1973 *J. Fluid Mech.* **59**, 721.

SEGUR, H. & HAMMACK, J. L. 1982 Long internal waves in layers of equal depth. Preprint.